CHEMICAL ENGINEERING TRANSACTIONS
VOL. 124, 2026
A publication of AIDIC
The Italian Association of Chemical Engineering
Online at www.cetjournal.it
Guest Editors: Marco Bravi, Antonio Marzocchella, Giuseppe Caputo

ISBN 979-12-81206-25-0; **ISSN** 2283-9216
DOI: 10.3303/CET26124035

Injectable Nanocomposite Hydrogels for Non-Critical Mandibular Fracture Repair

Federica Giuliano*, Simona Galvano, Federico Barrino, Emanuela Muscolino, Clelia Dispenza

Dipartimento di Ingegneria, Università degli Studi di Palermo, Viale delle Scienze 6, 90128 Palermo, Italy
federica.giuliano02@unipa.it

Injectable hydrogels are emerging material for the management of non-critical mandibular fractures. They have the capacity to enable minimally invasive interventions and conform to complex defect geometries. Within this framework, the present work focuses on the design of injectable nanocomposite hydrogels capable of avoiding soft-tissue collapse into mandibular bone defects, preserve geometry for later mineralization while delivering cues for bone regeneration. In particular, this work investigates injectable nanocomposite hydrogels based on k-carrageenan (kC) and guar gum (GG), reinforced with fluorapatite nanoparticles (FA NPs) as a biomimetic inorganic phase. FA NPs were synthesized via a sol–gel route and incorporated into the polysaccharide matrix at different loadings (0.5 % w/w, 1.0 % w/w), while the polymer composition was varied to modulate network properties. The resulting formulations were characterized in terms of rheological behaviour, morphology, and chemical structure. The hydrogels exhibited solid-like viscoelastic properties and a three-dimensional porous architecture, with FA NPs physically embedded within the polymer network. The results clearly demonstrate that the polymer ratio and nanoparticle content are key parameters governing the structural organization and viscoelastic response of the hydrogel, enabling tailored material properties.

1. Introduction

Periodontal diseases are among the most prevalent chronic conditions affecting the oral cavity, impacting up to 90% of the global population (Pihlstrom et al., 2005). They are characterized by progressive destruction of the periodontal supporting tissues, including the alveolar bone, which in advanced stages leads to compromised tooth stability and function, representing a significant clinical challenge. The pathological progression of periodontitis is driven by a persistent inflammatory microenvironment (Kinane et al., 2017), that promotes osteoclast-mediated bone resorption while simultaneously impairing bone regeneration. Periodontal inflammation and associated bone loss have also been linked to systemic conditions, and progressive alveolar bone resorption not only compromises oral health but can negatively affect the outcomes of subsequent orthodontic and restorative treatments (Kim and Amar, 2006). Conventional clinical approaches, including mechanical debridement, guided tissue regeneration, and bone grafting, can slow disease progression (Cortellini and Tonetti, 2015), but the effective restoration of periodontal bone defects remains difficult, particularly in irregular and confined anatomical sites such as periodontal pockets (Kaigler et al., 2011). In clinical practice, periodontal therapy is typically initiated with non-surgical approaches aimed at reducing inflammation through thorough mechanical debridement and plaque control, as surgical interventions are reserved for advanced or refractory cases. In this context, injectable biomaterials have emerged as promising alternatives to preformed grafts, owing to their minimally invasive delivery, adaptability to complex defect geometries, and ability to provide localized structural support (Li and Mooney, 2016). Injectable hydrogels, in particular, can act as temporary matrices capable of filling defects, maintaining a hydrated environment, and hosting bioactive inorganic phases (Xu et al., 2018). Their performance is governed by rheological behaviour, network stability, and degradation kinetics, which must be carefully tailored to the target application (Hoffman, 2002). Natural polysaccharides are widely explored as hydrogel-forming materials due to their biocompatibility, availability, and structural versatility (Giri et al., 2021). Among them, k-carrageenan is a sulphated polysaccharide known for its

Paper Received: 23 November 2025; Revised: 30 January 2026; Accepted: 9 March 2026
Please cite this article as: Giuliano F., Galvano S., Barrino F., Muscolino E., Dispenza C., 2026, Injectable Nanocomposite Hydrogels for Non-Critical Mandibular Fracture Repair, Chemical Engineering Transactions, 124, 205-210 DOI:10.3303/CET26124035

ability to form physically crosslinked networks with relatively high stiffness (Muscolino et al. 2022), while guar gum, a neutral galactomannan, contributes viscosity and flexibility to polymeric systems. The combination of kC and GG offers a modular strategy to tune injectability, viscoelastic response, and structural stability through compositional control, without the need for chemical crosslinking. Furthermore, the incorporation of bioinspired inorganic fillers represents an effective strategy to reinforce polymeric hydrogels and tailor their functional properties. Calcium phosphate–based nanoparticles are especially attractive in this context due to their compositional similarity to bone mineral. Among the different calcium phosphate phases, fluorapatite (FA) has received increasing attention, due to the fluoride substitution of hydroxyl groups with fluoride ions within the apatite lattice. In facts, fluoride incorporation has been associated with improved crystallinity, chemical stability, and resistance to dissolution. Moreover, fluoride-containing apatite influence bone remodelling processes and inflammatory bone resorption mechanisms, making them relevant candidates for periodontal-related applications (Liu et al., 2019). Based on these considerations, this work reports on the development and physicochemical characterization of injectable nanocomposite hydrogels composed of kC and GG, reinforced with FA NPs. The chosen nanoparticles were synthesized via a sol–gel process and incorporated into kC/GG hydrogel matrices with varying polymer ratios and nanoparticle loadings, with the aim of identifying formulations exhibiting suitable injectability and structural stability. The resulting systems were characterized by small-amplitude oscillatory rheology, scanning electron microscopy (SEM) for morphological assessment, and Fourier-transform infrared (FTIR) spectroscopy for chemical characterization of functional groups, in order to identify compositions with properties suitable for periodontal applications.

2. Experimental Section

2.1 Materials

Guar gum (Sigma-Aldrich) and k-carrageenan (Sigma-Aldrich) were used as polymeric components for hydrogel preparation. Ethanol (EtOH >99.5%, Sigma-Aldrich) and ultrapure water were employed as solvents. Calcium nitrate tetrahydrate ($Ca(NO_3)_2 \cdot 4H_2O$, Sigma-Aldrich), ammonium fluoride (NH_4F, Sigma-Aldrich), and triethyl phosphate (TEP, Molekula Group) were used as precursors for the synthesis of FA NPs.

2.2 Preparation of Fluorapatite Nanoparticles

FA NPs were synthesized using a sol–gel method. NH_4F was added to TEP dissolved in an ethanol–water mixture (95:5 v/v), maintaining a phosphorus-to-fluorine molar ratio (P/F) of 3. In a separate container, $Ca(NO_3)_2 \cdot 4H_2O$ was dissolved in ethanol after weighing the appropriate amount to ensure a molar ratio between calcium and fluorine of Ca:F = 5:1. Both solutions were vigorously stirred for 24 h at room temperature and then the calcium-containing solution was slowly added to the phosphorus-containing solution. The resulting sol was mixed at room temperature for 72 h and then aged for an additional 24 h. The obtained gel was dried at 70 °C for 3 days and subsequently heat-treated at 550 °C for 1 h. After thermal treatment, the material was gently ground using a pestle and mortar to obtain a fine powder.

2.3 Preparation of Hydrogels

kC aqueous solutions with polymer concentrations of 1.0 % w/w (kC1) and 2.0 % w/w (kC2) were prepared by weighing and dispersing the polymer powder in ultrapure water and heating the mixture to 80 °C under continuous stirring until complete solubilization was achieved. FA NPs were subsequently added to the kC solutions at concentrations of 0.5 % w/w (FNp05) and 1.0 % w/w (FNp1), and the resulting suspensions were stirred for 1 h to promote homogeneous nanoparticle dispersion. In parallel, GG solutions with a concentration of 2.0 % w/w (GG2) were prepared by dispersing the polymer in ultrapure water at room temperature under continuous stirring. The kC/FA NPs suspensions were then combined with the GG solution to obtain four formulations, named as kC1GG2FNp05, kC2GG2FNp05, kC1GG2FNp1, and kC2GG2FNp1. The mixtures were maintained in a water bath at 80 °C for 2 h under magnetic stirring to ensure effective component incorporation and formulation homogeneity. After mixing, the solutions were allowed to cool naturally to room temperature, inducing a sol–gel transition and resulting in the formation of injectable hydrogels.

2.4 Fourier Transform Infrared (FTIR) Spectroscopy

FTIR spectroscopy was employed to investigate the chemical structure and interactions within the nanocomposite hydrogels. Spectra were acquired using a PerkinElmer FT-IR/NIR Spectrum 400 spectrophotometer equipped with an AIM-8800 infrared microscope (Shimadzu, Tokyo, Japan). Measurements were performed at a resolution of 4 cm^{-1} with 64 scans per sample, an incidence angle of 30°, and a spectral range from 400 to 4000 cm^{-1}.

2.5 Scanning Electron Microscopy (SEM)

The morphology of the hydrogels was analysed using a FEI Quanta 200 FEG scanning electron microscope operating at an accelerating voltage of 10 kV. Samples were frozen in liquid nitrogen and subsequently freeze-dried to remove water. The dried samples were fractured to expose cross-sectional surfaces, mounted on aluminium stubs using graphite adhesive, and sputter-coated with gold using a JFC-1300 sputter coater (JEOL) for 120 s prior to imaging.

2.6 Rheological Characterization

Rheological measurements were performed using stress-controlled rheometers (HR-20, TA Instruments) equipped with a crosshatched Peltier plate geometry with a diameter of 20 mm.

2.6.1 Temperature ramp measurement

The gelation behaviour of the hydrogel systems was studied by performing oscillatory rheometric measurements conducted at fixed strain value, chosen for each formulation from a strain sweep test at 1 Hz, to test the material within its linear viscoelastic region. The hydrogel solutions were loaded directly onto the bottom plate of rheometer and were surrounded by a thin layer of silicon oil to prevent water evaporation. The temperature was decreased from 80 °C to 25 °C at a ramp rate of 3 °C/min, with the oscillation frequency set to 1 Hz.

2.6.2 Frequency Sweep Test

Frequency sweep measurements were performed at a fixed strain value selected within the linear viscoelastic region, as determined from a strain sweep tests conducted at 1 Hz. The frequency was varied from 0.1 Hz to 10 Hz at a constant temperature of 37 °C. Samples were loaded directly onto the rheometer bottom plate prior to testing.

3. Results and discussion

The physicochemical and rheological properties of the kC/GG hydrogels reinforced with FA NPs were systematically investigated to assess the effect of polymer composition and nanoparticle loading on network structure and viscoelastic behaviour. The results are presented by combining chemical, morphological, and rheological analyses to provide a comprehensive and coherent description of the material properties.

3.1 FTIR analysis

FTIR spectroscopy was employed to investigate the chemical structure of the hydrogels and the effect of FA NPs incorporation. Figure 1a reports the FTIR spectra of all hydrogel formulations, with the spectrum of FA NPs used as reference. The FA NPs exhibit characteristic PO_4^{3-} bands, with intense stretching peaks around 1087 cm^{-1} and 1043 cm^{-1} and bending peaks at 601 cm^{-1} and 562 cm^{-1}, while the absence of hydroxyl-related adsorptions confirms fluoride substitution in the apatite lattice.

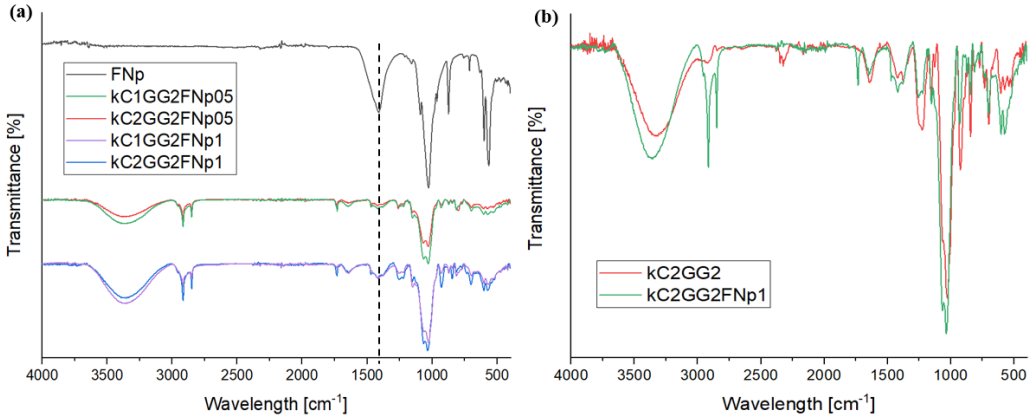

Figure 1: FTIR spectra of (a) kC/GG hydrogels with different polymer compositions and FA NPs contents (0, 0.5 % w/w and 1.0 % w/w), compared with FA NPs; (b) kC2GG2 hydrogel and the corresponding nanocomposite systems containing 1.0 % w/w FA NPs.

All hydrogel spectra display the characteristic features of polysaccharide-based hydrogels, including a broad O–H stretching band in the 3200–3500 cm^{-1} region, C–H stretching vibrations around 2900 cm^{-1}, and intense bands between 1000 cm^{-1} and 1150 cm^{-1} associated with C–O–C and C–O stretching modes of the

polysaccharide backbone. The presence of sulphate ester groups from kC is confirmed by bands in the 1220–1260 cm^{-1} range. To better highlight the effect of FA Figure 1b compares the FTIR spectra of the kC2GG2 hydrogel with the corresponding systems containing 1.0 % w/w FA NPs. In these formulations, some spectral changes can be observed, including a narrowing of the O–H stretching band and the increased definition of absorption features below 3000 cm^{-1}, attributed to C–H stretching vibrations. In addition, weak contributions in the 600–500 cm^{-1} region become more evident, consistent with PO_4^{3-} bands of fluorapatite. Overall, the FTIR results indicate that FA NP incorporation at 1.0 % w/w leads to detectable modifications of the hydrogel spectral profile, while preserving the chemical structure of the polysaccharide network, consistent with physical embedding of the inorganic phase.

3.2 Morphological evaluation

The internal morphology of the hydrogels was investigated by SEM. Representative micrographs of the base hydrogels and nanocomposite systems are shown in Figures 2. The base formulations exhibited a layered, lamellar microstructure, typical of physically crosslinked polysaccharide networks formed via thermally induced gelation. The pores are highly anisotropic and predominantly extend within the interlamellar regions. Increasing the kC content from 1.0 % w/w to 2.0 % w/w results in a more randomly porous morphology, with reduced voids size, indicating a higher density of physical junctions. The incorporation of FA NPs induced drastic changes in the hydrogel microstructure. For both kC1GG2 and kC2GG2 systems, the addition of 0.5 % w/w and 1.0 % w/w FA NPs led to a progressive densification of the hydrogel network. Individual nanoparticles were not directly observable due to their small size and embedding within the polymer matrix; however, their influence on the microscale organization of the hydrogel network suggests that they, or potentially the released Ca^{2+} ions, act as crosslinking agents.

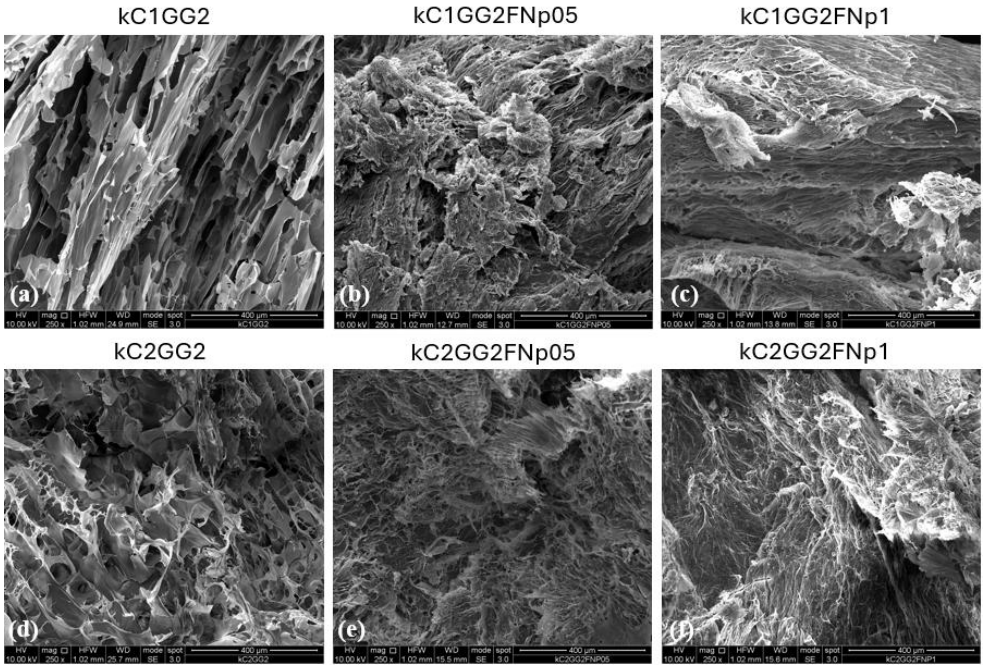

Figure 2: SEM micrographs of kC1GG2 (a, b, c) and kC2GG2 (d, e, f) systems with and without FA NPs at 250x magnification.

3.3 Rheological behaviour

Rheological characterization was carried out to evaluate the thermoresponsive behaviour, mechanical stability, and injectability-related properties of the hydrogels.Temperature sweep experiments under cooling conditions, shown in Figure 3, were conducted to evaluate the sol–gel transition behaviour of the hydrogels. Independently of polymer composition and nanoparticle content, all systems exhibited a clear evolution of viscoelastic properties upon cooling, reflecting the progressive formation of physically crosslinked polysaccharide networks. In pristine systems, a predominantly viscous behaviour was observed at higher temperatures, as indicated by G″ > G′. As the temperature was decreased, a crossover between G′ and G″ occurred, after which G′ became dominant, marking the transition from a sol-like to a gel-like state. This behaviour is consistent with the phenomenon of thermally induced physical gelation. The incorporation of FA NPs significantly affected the sol–gel transition temperature behaviour, with the G′/G″ crossover that occurs at higher temperatures. The presence

of nanoparticles resulted in an earlier dominance of the elastic component during cooling, indicating a lower sol–gel transition temperature compared to the corresponding nanoparticle-free hydrogels. This behaviour suggests that nanoparticles actively contribute to network formation, likely by acting as physical crosslinking points or reinforcing elements that restrict chain mobility. Comparing the two polymer compositions, hydrogels with higher kC content display increased thermal stability, maintaining higher modulus values across the investigated temperature range.

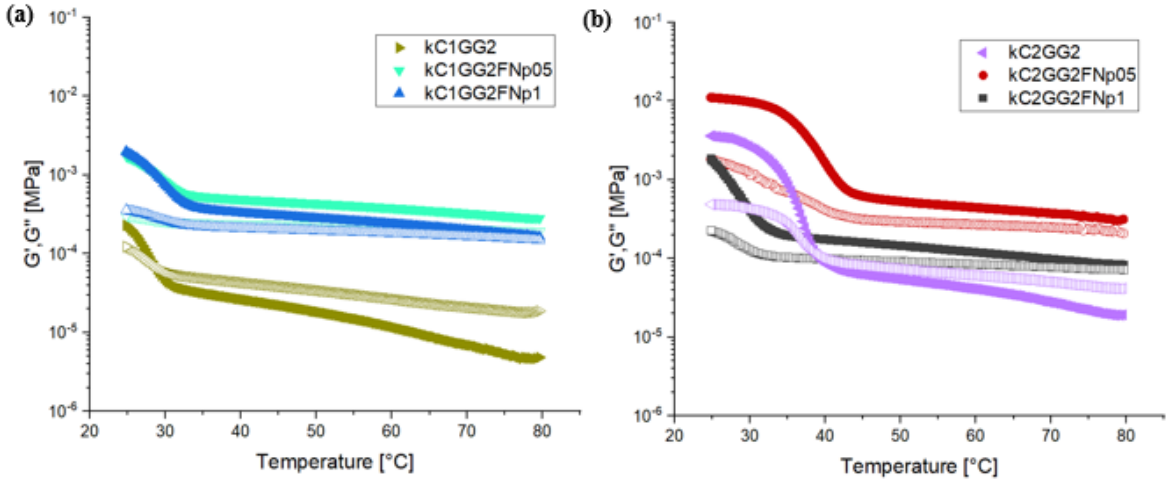

Figure 3: Storage modulus (G', filled symbols) and loss modulus (G", empty symbols) as a function of Temperature for kC/GG hydrogels with different kC contents (1.0 % w/w (a) and 2.0 % w/w (b)) and FA NPs loadings.

The kC2GG2 formulation was identified as the most suitable candidate for further analysis based on the temperature-dependent rheological behaviour and morphological observations. This system combines a well-defined sol–gel transition at experimentally accessible temperatures with higher post-gelation mechanical stability and a porous microstructure that is preserved even in the presence of FA NPs. These features are particularly relevant for injectable applications, where the material must be easily handled in the sol-state and rapidly form a mechanically stable gel in situ after administration. Therefore, frequency sweep measurements were selectively performed on kC2GG2-based hydrogels to evaluate their viscoelastic stability under dynamic conditions. As shown in Figure 4, all formulations exhibited a predominantly elastic response over the explored frequency range, with G′ consistently exceeding G″, indicating stable gel-like networks. The weak frequency dependence of both moduli indicates the formation of physically crosslinked networks with good mechanical stability under dynamic conditions. The incorporation of FA NPs further enhanced G′ and G″ values, consistent with a reinforcing effect of the inorganic phase and/or released Ca^{2+} cations.

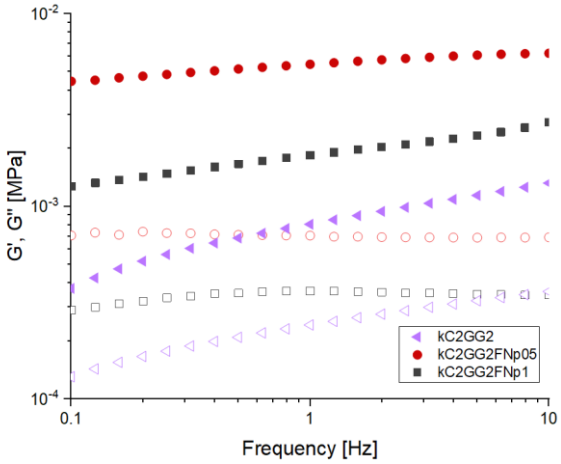

Figure 4: Storage modulus (G', filled symbols) and loss modulus (G", empty symbols) as a function of frequency for κC2GG2 hydrogels with and without FA NPs contents.

4. Conclusions

Injectable nanocomposite hydrogels based on kC and GG reinforced with FA NPs were successfully developed. The combined use of the two polysaccharides enabled the formation of thermosensitive hydrogel networks which exhibited solid-like viscoelastic behaviour under physiological conditions, with properties like their extrudability that could be effectively tuned through polymer composition, rendering them adaptable for use in treatments involving non-critical bone defects. FTIR spectroscopy provided evidence that FA NPs were physically embedded within the hydrogel network. SEM analysis revealed a porous architecture, whose organization is influenced by both polymer composition and NPs content. Temperature-dependent rheological analysis demonstrated that all formulations undergo a sol–gel transition upon cooling, while FA NPs promote earlier network formation. Among the investigated compositions, the kC2GG2 formulation was selected as the optimal candidate because it maintained a more porous and less dense structure, while exhibiting the most suitable balance between injectability in the sol state and mechanical stability after gelation, maintaining an elastic-dominated response at physiological temperature. Frequency sweep measurements performed on kC2GG2 systems confirmed the formation of stable gel-like networks under dynamic conditions, with nanoparticle addition providing moderate mechanical reinforcement without compromising viscoelastic balance. The results of the study indicate that the kC/GG nanocomposite hydrogels, particularly the kC2GG2 formulation, have the potential to serve as promising injectable systems capable of in situ gelation and mechanical stabilization. Subsequent studies will concentrate on the quantification of ion release and biological assessment to further validate their regenerative potential.

References

Cortellini P., Tonetti M. S., 2015, Clinical concepts for regenerative therapy in intrabony defects, Periodontology 2000, 68, 282–307.

Giri S., Dutta P., Kumarasamv D., Giri T. K., 2021, Natural polysaccharides: Types, basic structure and suitability for forming hydrogels, Plant and Algal Hydrogels for Drug Delivery and Regenerative Medicine, 1-35.

Hoffman A. S., 2002, Hydrogels for biomedical applications, Advanced drug delivery reviews, 54, 3–12.

Kaigler D., Avila G., Wisner-Lynch L., Nevins M. L., Nevins M., Rasperini G., Lynch S. E., Giannobile W. V., 2011, Platelet-derived growth factor applications in periodontal and peri-implant bone regeneration, Expert opinion on biological therapy, 11, 375–385.

Kim J., Amar S., 2006, Periodontal disease and systemic conditions: a bidirectional relationship, Odontology 94, 10-21.

Kinane D., Stathopoulou P., Papapanou P., 2017, Periodontal diseases, Nature Reviews Disease Primers, 3.

Li J., Mooney D. J., 2016, Designing hydrogels for controlled drug delivery, Nature reviews Materials, 1, 16071.

Liu S., Zhou H., Liu H., Ji H., Fei W., Luo E., 2019, Fluorine-contained hydroxyapatite suppresses bone resorption through inhibiting osteoclasts differentiation and function in vitro and in vivo, Cell Proliferation, 52.

Muscolino E., Di Stefano A.B., Trapani M., Sabatino M.A., Giacomazza D., Alessi S., Cammarata E., Moschella F., Cordova A., Toia F., Dispenza C., 2022b, κ-Carrageenan and PVA blends as bioinks to 3D print scaffolds for cartilage reconstruction, International Journal of Biological Macromolecules, 222, 1861–1875.

Pihlstrom B. L., Michalowicz B. S., Johnson N. W., 2005, Periodontal diseases, Lancet, 366, 1809–1820.

Xu X., Gu Z., Chen X., Shi C., Liu C., Liu M., Wang L., Sun M., Zhang K., Liu O., Shen Y., Lin C., Yang B., Sun H., 2019, An injectable and thermosensitive hydrogel: Promoting periodontal regeneration by controlled-release of aspirin and erythropoietin, Acta Biomaterialia, 86, 235-246